Fluctuation correlation models for receptor immobilization

B. Fourcade*
Laboratoire Interdisciplinaire de Physique, UMR-CNRS 5588, Université Grenoble Alpes and Institut Albert Bonniot, INSERM U1209-CNRS 5309, Grenoble, France
(Received 16 September 2017; published 11 December 2017)

Nanoscale dynamics with cycles of receptor diffusion and immobilization by cell-external-or-internal factors is a key process in living cell adhesion phenomena at the origin of a plethora of signal transduction pathways. Motivated by modern correlation microscopy approaches, the receptor correlation functions in physical models based on diffusion-influenced reaction is studied. Using analytical and stochastic modeling, this paper focuses on the hybrid regime where diffusion and reaction are not truly separable. The time receptor autocorrelation functions are shown to be indexed by different time scales and their asymptotic expansions are given. Stochastic simulations show that this analysis can be extended to situations with a small number of molecules. It is also demonstrated that this analysis applies when receptor immobilization is coupled to environmental noise.

DOI: 10.1103/PhysRevE.96.062403

I. INTRODUCTION

Image correlation microscopy typically measures correlation functions for concentration fluctuations in a small volume of excitation [1,2]. For such volumes with a small number of tagged molecules, fluctuations of the fluorescence are distinguishable from averages. Analyzing these fluctuations through temporal correlations allows determining the time course of the biochemical reactions occurring in the illuminated focus. Because of these developments, these methods have been intensively applied in cell biology where immobilization and signaling are generic questions [3,4]. In particular, the spatiotemporal dynamics of receptors at adhesive sites have been characterized using a wide range of techniques to investigate key events taking place in adhesive sites [5–11]. One advantage of the fluctuation microscopy techniques is that they give information about the binding and unbinding of receptors to intracellular components or to extracellular factors, these processes being at the origin of the mechanoregulation of cell signaling [12,13].

This paper revisits the problem of calculating noise correlation functions for a 2D-diffusing receptor binding to and unbinding from an immobile substrate, i.e., an extra or intracellular factor; see Fig. 1. Integrins receptors cycling between different affinity states are prototypical receptors [12]. They link the extracellular microenvironment to the intracellular cytoskeleton-associated partners in adhesive zones, which are loosely organized into clusters [5,9–11,14]. These references point out that the nanoscale dynamics of integrin receptors in these adhesive zones is characterized by cycles of 2D diffusion and immobilization with a large distribution of residence times [9]. From the theoretical point of view, this problem has been studied in the past; see Ref. [15] and references therein. Working in the limit of large excess of ligands, these references assume different asymptotic regimes where either diffusion or reaction dominates so that the problem is computationally simplified. The present paper goes one step further, both from the analytical and numerical point of view. It gives a more precise analysis in all regimes and derives simple exact results valid in all cases in the small time limit. The role of boundary conditions is demonstrated for experimentally relevant systems where adhesive disks are in contact with a reservoir of freely diffusing particles and, to avoid introducing artifacts, situations where neither receptors nor ligands are in excess are considered. This approach is supported by analytical and numerical calculations. Stochastic simulations sampling all the configuration space are shown to give reliable results for the autocorrelation functions. This allows us to study more complex situations for receptors cycling between different conformational states and where an environmental noise induces large spatial and temporal fluctuations in the number of ligands. The preceding analysis also applies in this case and it is shown that the dynamics of immobilization sites can be a powerful mechanism to regulate cell adhesive properties.

In the limit where ligands are in excess, the findings are summarized in Fig. 2 where the diffusion time τ_D is defined for a sampled region of area πw^2. Using this time as a reference time scale for the effective binding, $k_b^\star$, and unbinding, k_u, rates, the product $(k_b^\star + k_u)\tau_D = 1$ compares the two characteristic times where the correlations regress either via reaction or diffusion. Below this line, reaction and diffusion are not truly separable. Analytical expressions for the autocorrelation function are given in Eqs. (22)–(25) for parameters below this line. In the sufficiently low binding rate regime, the signature of this regime is a hybrid algebraic decay in the short limit combined with a long exponential decay due to reaction in the long time limit. I give an exact result valid in the very small time scale limit for all regimes, see Ref. (19), as well as the asymptotic forms for the autocorrelation functions. Stochastic simulations show that this analysis still holds in the limit where the ligands are not in excess if the effective rate constants are properly defined.

The plan of this paper follows this introduction and is followed by appendices with mathematical details.

II. THE MODEL

To introduce the notations, let I be a receptor cycling between two conformational states $\mathrm{I}_\uparrow$ and $\mathrm{I}_\downarrow$,

$$\mathrm{I}_\uparrow \underset{k_-}{\overset{k_+}{\rightleftarrows}} \mathrm{I}_\downarrow, \tag{1}$$

*Bertrand.Fourcade@univ-grenoble-alpes.fr

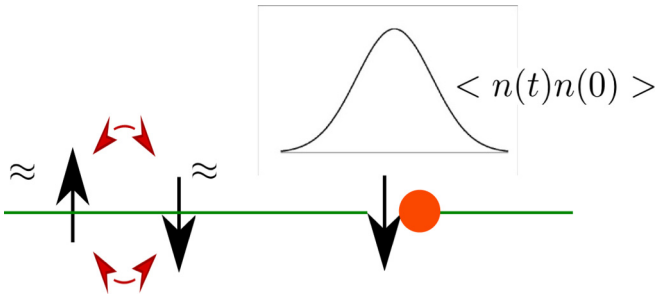

FIG. 1. Receptors cycling between two conformational states diffuse on a two-dimensional membrane and they interact with immobilized ligand. Illumination through a Gaussian point-spread function (PSF) allows us to count the total number of receptors in the PSF region and to evaluate their time correlation functions.

where the down arrow symbolizes the extended conformation characteristic of integrin receptor in its active conformation. Let us assume that receptors can interact with a fixed ligand L and form a complex I−L via a reversible interaction. This reaction occurs only when the receptor is in its down high-avidity conformation $I_\downarrow$,

$$I_\downarrow + L \underset{k_u}{\overset{k_b}{\rightleftarrows}} I - L. \tag{2}$$

Otherwise stated, the affinity of $I_\uparrow$ with L is so small that only reaction is considered [Eq. (2)]. The constants $k_{b,u}$, b standing for binding and u for unbinding, are rate constants. In both states, $I_{\uparrow,\downarrow}$, the receptor I diffuses on the membrane with diffusion coefficient $D = D_{\uparrow,\downarrow}$. Typically $I_\uparrow$ represents an integrin in its nonactivated state and $I_\downarrow$ an integrin in its activated state with a much larger affinity for an outside

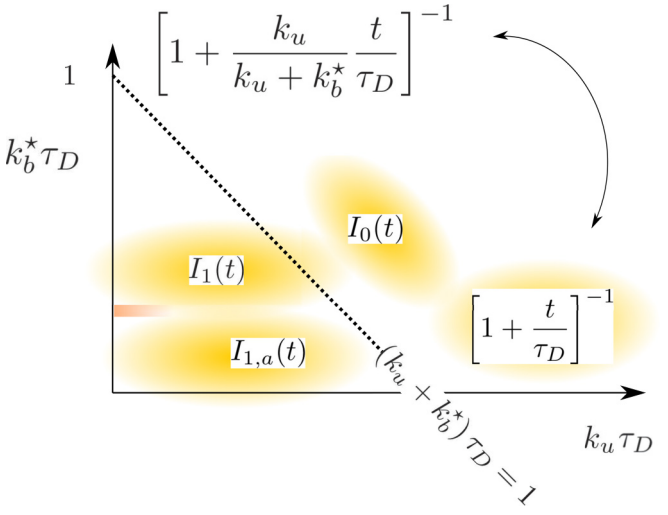

FIG. 2. Diagram for the receptor correlation function $I(t)$ for different sets of parameters. The two rate constants, $k_b^\star$ and k_u, b for binding and u for unbinding, are renormalized by the diffusion time. The slanted doted line corresponds to the boundary above which reaction is faster than diffusion. The three functional forms $I_0(t)$, $I_1(t)$, and its asymptotic form $I_{1,a}(t)$, are defined in the text; see Eqs. (21), (24), and (25). The effective diffusion limit matches the free diffusion for large unbinding rates k_u as indicated by the arrows.

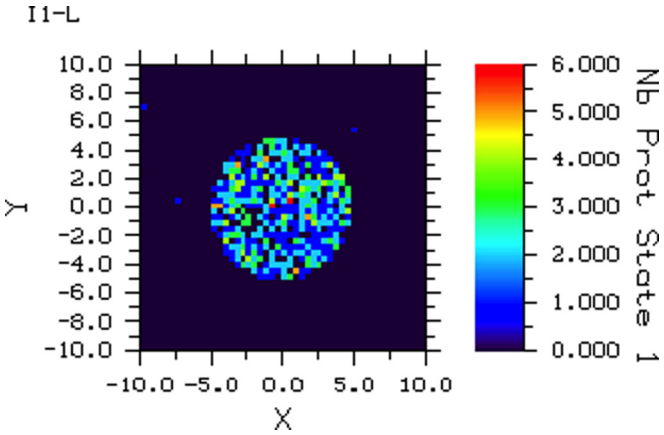

FIG. 3. Snapshot of a stochastic simulation. This plot is a color density plot corresponding to ligated receptors I−L in each compartment. The central disk corresponds to the adhesive region where the ligands are immobilized. Outside this region, the receptors freely diffuse without interacting with ligands and can exchange with a reservoir at the boundary of the square windowpane. The region S of width w for computing the correlation functions is inside the adhesive disk. The mean density of freely diffusing receptors inside and outside the disk are the same because of equal diffusion constants.

ligand, i.e., fibronectin, or an inside ligand, i.e., a cytoskeleton element.

We work with surface densities $n_\downarrow, n_\uparrow, n_b$, and l for activated, nonactivated, bound receptors, and free ligands, respectively. Assuming for the moment that most of the integrins are in their activated state, the model is written as a system of first-order kinetic equations,

$$\partial_t n_\downarrow = D\Delta n_\downarrow - k_b l n_\downarrow + k_u n_b, \tag{3}$$

$$\partial_t n_b = +k_b l n_\downarrow - k_u n_b, \tag{4}$$

where Δ is the two-dimensional Laplacian operator for diffusion. The usual mean-field approximation assumes negligible ligand fluctuations, so that one can define the effective rate constant using the average l_0 with $k_b^\star = k_b l_0$. For an adhesive disk in contact with a reservoir of diffusing receptors, the large ligand limit poses, however, problem in the long time residence limit, since all receptors tend to accumulate at the adhesive- non-adhesive boundary. In what follows, it will be, therefore, appropriate to consider a finite density of ligands in this regime.

The system of Eqs. (3) and (4) is well posed when boundary conditions are specified. In what follows, I will use two boundary conditions to calculate the fluctuations around the mean. The first is the usual reflective, or zero flux, boundary condition with a fixed number of molecules. The second is the open boundary condition where receptors are in contact with a reservoir with a given average density $n_\downarrow$; see Fig. 3. This condition applies to heterogeneous systems where experiments probe only adhesive sites in contact with the surrounding cell membrane. Stationary solutions for the two cases differ, since the population of freely diffusing receptors in the adhesive disk is set by the density outside the disk when the diffusion constants are equal. For reflective boundary conditions, the

fractional population of freely diffusive particles is determined by their interaction with the ligands and the autocorrelation functions have different properties in the two cases.

The observable quantity in FCS-like experiments corresponds to the weighted correlation function,

$$I(t) = \iint_{w^2} d\mu(\mathbf{x}) d\mu(\mathbf{x}') \langle \delta n(\mathbf{x},t) \delta n(\mathbf{x}',0) \rangle, \tag{5}$$

where the total density contributes to the fluorescence volume:

$$\delta n(\mathbf{x},t) = \delta n_{\downarrow}(\mathbf{x},t) + \delta n_b(\mathbf{x},t). \tag{6}$$

The symbol $\langle \ldots \rangle$ refers to the average over the stationary distribution corresponding to the problem defined in Eqs. (3) and (4).

The long time limit of the weighted correlation functions in Eq. (5) does not depend on the conditions of illumination. It is usual to take a Gaussian average for the point-spread function as

$$d\mu(\mathbf{x}) = e^{-2\mathbf{x}^2/w^2} d^2x. \tag{7}$$

We will see, however, that the short time limit depends on the geometry of the illuminated area. Using the Lax and Mengert argument [16], correlation functions probe the conditional probability to find a random walker in the illuminated region at time t given that it was in that region at time $t = 0$. When t is small compared with all other times, the correlation function probes only random walkers at the periphery of the illuminated region and thus the tails of the Gaussian. It is therefore instructive to compare the Gaussian measure with the strong cutoff measure,

$$d\mu(\mathbf{x}) = \Theta(w^2 - \mathbf{x}^2), \tag{8}$$

where $\Theta(r)$ is the step function, $\Theta(r) = 1$ if $r > 0$ and 0, otherwise. The case of Eq. (7) corresponds to the classical Gaussian illuminated case and Eq. (8) for the sharp circular illuminated measure, the latter case being appropriate when averaging is done over a region larger than the Gaussian point-spread function.

III. SUMMARY OF THE METHOD

To compute Eq. (5), I follow the Onsager's regression hypothesis, which states that microscopic fluctuations cannot be distinguished from macroscopic regressions toward equilibrium when the system is initially prepared in a nonequilibrium state [17]. If we define $n = n_{\downarrow} + n_b$, we have

$$\langle \delta n(\mathbf{x},0) \delta n(\mathbf{x}',0) \rangle = \langle \delta n_{\downarrow}^2 \rangle \delta^{(2)}(\mathbf{x} - \mathbf{x}') + \langle \delta n_b^2 \rangle \delta^{(2)}(\mathbf{x} - \mathbf{x}') + 2\langle \delta n_{\downarrow} \delta n_b \rangle \delta^{(2)}(\mathbf{x} - \mathbf{x}'), \tag{9}$$

where $\langle \delta n_{\downarrow}^2 \rangle$, $\langle \delta n_b^2 \rangle$ satisfy Poisson's statistic with $\langle \delta n_{\downarrow,l}^2 \rangle = n_{\downarrow,l}$. Because $n_{\downarrow}$ is a diffusing field, the cross-correlation $\langle \delta n_{\downarrow} \delta n_b \rangle$ is assumed to be zero.

As usual, Eqs. (3) and (4) are solved by Fourier transforming in space,

$$\delta \tilde{n}_{\downarrow,l}(\mathbf{k},t) = \frac{1}{(2\pi)^2} \int d^2x \, \delta n_{\downarrow,l}(\mathbf{x},t) e^{-i\mathbf{k}.\mathbf{x}}, \tag{10}$$

where

$$\langle \delta \tilde{n}_{\downarrow,l}(\mathbf{k},t) \delta \tilde{n}_{\downarrow,l}(\mathbf{k}',t) \rangle = (2\pi)^2 \langle \delta n_{\downarrow,l}^2 \rangle \delta^{(2)}(\mathbf{k} + \mathbf{k}'). \tag{11}$$

As a result, the macroscopic fluctuations $\Delta \tilde{n}_{\pm}(\mathbf{k},t)$ obey the following ordinary differential equation:

$$\begin{pmatrix} \partial_t \delta \tilde{n}_{\downarrow}(\mathbf{k},t) \\ \partial_t \delta \tilde{n}_b(\mathbf{k},t) \end{pmatrix} = \begin{pmatrix} -D\mathbf{k}^2 - k_b^{\star} & k_u \\ k_b^{\star} & -k_u \end{pmatrix} \begin{pmatrix} \delta \tilde{n}_{\downarrow}(\mathbf{k},t) \\ \delta \tilde{n}_b(\mathbf{k},t) \end{pmatrix}. \tag{12}$$

Given initial conditions, we write the solution as

$$\begin{pmatrix} \delta \tilde{n}_{\downarrow}(\mathbf{k},t) \\ \delta \tilde{n}_b(\mathbf{k},t) \end{pmatrix} = \begin{pmatrix} \alpha_{11} & \alpha_{12} \\ \alpha_{21} & \alpha_{22} \end{pmatrix} \begin{pmatrix} \delta \tilde{n}_{\downarrow}(\mathbf{k},0) \\ \delta \tilde{n}_b(\mathbf{k},0) \end{pmatrix}, \tag{13}$$

where $[\alpha]$ in Eq. (13) is a matrix with coefficients depending on the wave vector $\mathbf{k}$ and on the time t. The matrix $[\alpha]$ is found by using the eigenvectors and the eigenvalues of Eq. (12); see the Appendix.

As usual, it is more convenient to work with dimensionless quantities. We define $q = w/2k$ and find for the Gaussian case

$$I(t) = \frac{\pi}{4} w^2 \int_0^{\infty} q dq \, e^{-q^2} \big[(\alpha_{11} + \alpha_{21}) \langle \delta n_{\downarrow}^2 \rangle + (\alpha_{12} + \alpha_{22}) \langle \delta n_b^2 \rangle \big]. \tag{14}$$

We have $\langle \delta n_{\downarrow}^2 \rangle = \langle n_{\downarrow} \rangle$ and $\langle \delta n_b^2 \rangle = \langle n_b \rangle$, and it is useful to rewrite Eq. (14) as a weighted linear combination of $\exp[\Lambda_{\pm}(q)t]$ exponentials as

$$\sum_{\pm} \int_0^{\infty} q dq \, e^{-q^2} C_{\pm}(q) e^{\Lambda_{\pm}(q)t} = I_+(t) + I_-(t), \tag{15}$$

where $C_{\pm}(q)$ satisfies an equivalent condition of mass conservation as

$$C_+(q) + C_-(q) = 1. \tag{16}$$

Computing the integral Eq. (15) in all regimes is straightforward from the numerical point of view. It is, however, interesting to derive its asymptotic forms in different asymptotic limits. The usual procedure is to retain the dominant eigenvalue $\Lambda_+(q)$ in the small q limit and to neglect all variations for the $C_{\pm}(q)$'s. This leads to the so-called effective diffusion regime with

$$I(t)/I(0) \simeq \left[1 + \frac{k_u}{k_u + k_b^{\star}} \frac{t}{\tau_D} \right]^{-1}, \tag{17}$$

where $k_u/(k_u + k_b^{\star})$ is the fraction of unbound receptors. As seen in the Appendix, this usual result is only valid if two conditions are met. First, this fraction has to be large. Second, the critical wave vector

$$q_i^{\star} = [\tau_D (k_b^{\star} + k_u)]^{1/2} \tag{18}$$

must be larger than one so that the $C_{\pm}(q)$'s vary slowly on the scale set by the Gaussian factor, $\exp(-q^2)$. In this case, they can be safely approximated as constant. Plotting $C_{\pm}(q)$ as done in Fig. 4 demonstrates that this condition for the effective diffusion regime is equivalent to $k_b^{\star} \tau_D \gg 1$ as shown in Fig. 2.

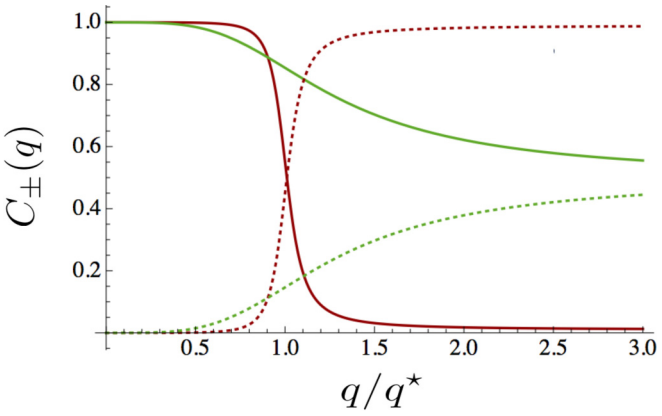

FIG. 4. Plot of $C_+(q)$ (continuous lines) and $C_-(q)$ (dotted lines) for large and small fraction of bound receptors, $k_u/(k_u + k_b^\star) = 0.99$ and 0.5. Functions are steplike in the limit of small bound fraction with a critical wave vector $q_i^\star$; see Eq. (18).

IV. AN EXACT RESULT

To analyze Eq. (15) further for reflective boundary conditions, it is useful to give an exact result valid in all regimes of Fig. 2 and probing the very short time limit of the correlation functions. Taking the derivative under the integral sign, calculation shows that the slope is proportional to the averaged fraction of freely diffusing receptors,

$$I'(0)/I(0) = -\frac{k_u}{k_b^\star + k_u}\frac{1}{\tau_D}. \tag{19}$$

In other words, decreasing the bound fraction of receptors shifts downwards the correlation function so that diffusion and reaction cannot be considered as truly separable processes even in the short time limit. This result is clearly validated in the so-called effective diffusion limit but it holds true in general. For open boundary conditions, the same calculation shows

$$I'(0)/I(0) = -\frac{1}{\tau_D}. \tag{20}$$

Equations (19) and (20) are signature of a Gaussian illumination. For the circular case with a sharp boundary, the slope is minus infinity; see the Appendix. Curves are, therefore, shifted downwards as seen from the following argument due to Lax and Mengert [16]; see Fig. 5. Correlation functions are equivalent to conditional probabilities that a random walker leaving the illuminated region at time $t = 0$ is observed in this region at a time t later. For small times t, only random walkers near the boundary can influence this probability and the return statistics depend on the way this boundary is defined.

V. ASYMPTOTIC FORMS OF THE AUTOCORRELATION FUNCTION $I(t)$

Our results are more easily summarized if we define the intermediate function $I_0(t)$ via its integral representation,

$$I_0(t) = \int_0^\infty dq\, q e^{-q^2 + \Lambda_+(q)t}. \tag{21}$$

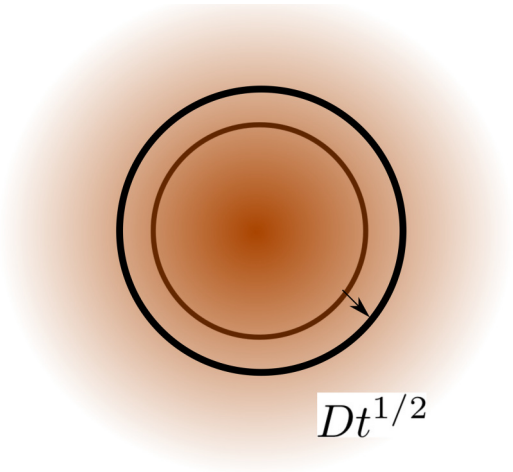

FIG. 5. This figure illustrates the Lax and Mergert argument [16] in the pure diffusion limit where the correlation $I(t)/I(0)$ is interpreted as the conditional probability for a random walker leaving the illuminated region of width w at time $t = 0$ to be observed in this region at a time t later. The diffusion length is $(Dt)^{1/2}$. When t is small, $I(t)/I(0)$ probes only random walkers at the boundary of the illuminated region. In the circular case where the boundary is much more sharply defined than in the Gaussian point-spread function case, one expects correlations to behave differently in the small time limit.

Explicit representations of Eq. (21) together with asymptotic forms are given in the Appendix. These results are valid for both boundary conditions with effective rate constants if necessary. In summary, we find the following cases:

(1) For $\tau_D(k_u + k_b^\star) \geqslant 1$, we find

$$I(t) \approx I_0(t). \tag{22}$$

Compared with brute force numerical calculations, this asymptotic form holds even on the line $(k_b^\star + k_u)\tau_D = 1$ of Fig. 2; see case (c) of Figs. 6 and 7. Using the asymptotic forms of Eq. (21), we recover the effective diffusion limit with a characteristic time

$$\frac{1}{\tau_{\text{eff}}} = \frac{k_u}{k_b^\star + k_u}\frac{1}{\tau_D} \tag{23}$$

and the pure diffusion limit when the unbinding rate k_u dominates over the binding rate $k_b^\star$.

(2) Below the dotted diagonal of Fig. 2, i.e., for $\tau_D(k_u + k_b^\star) \leqslant 1$, we find

$$I(t) \approx I_1(t) \equiv \frac{k_b^\star}{k_u + k_b^\star} I_0(t) + \frac{k_u}{k_u + k_b^\star}\frac{1}{1 + t/\tau_D}, \tag{24}$$

which is in general valid for sufficiently large t; see case (d) of Figs. 6 and 7. In the small t regime, it suffices to use condition Eq. (19).

When $k_b^\star \tau_D \ll 1$, Eq. (24) still holds; see cases (a) and (b) of Figs. 6 and 7. Algebra can be simplified further in this limit,

$$I(t) \approx I_{1,a}(t) = \frac{1}{1 + t/\tau_D} + \frac{k_b^\star}{k_u + k_b^\star}\frac{t/\tau_D}{1 + t/\tau_D}\exp[-k_u t], \tag{25}$$

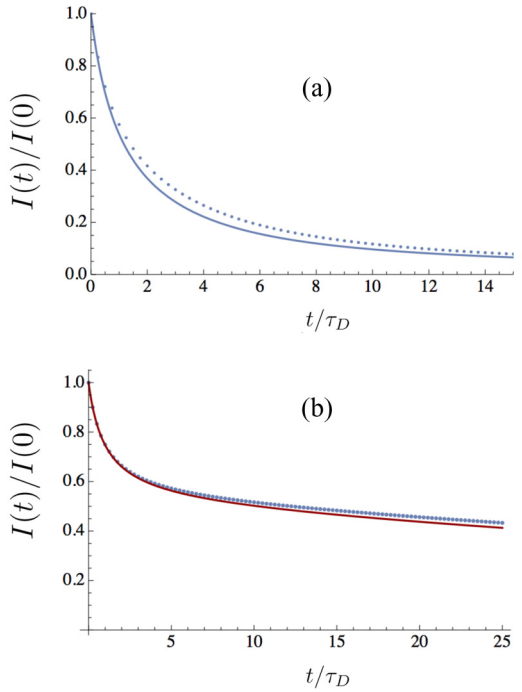

FIG. 6. Plots of the autocorrelation functions in different regimes according to Fig. 2. In all cases, the dotted line corresponds to the numerical evaluation of $I(t)/I(0)$ versus t/τ_d, $\tau_d = 1$, using Eq. (15). In case (a), $k_b\tau_D = 0.1$, $k_u\tau_D = 0.5$ and in case (b), $k_b = 0.01$, $k_u = 0.01$. These two limit cases correspond to the regime where $I(t)$ is well approximated by the asymptotic form $I_{1,a}(t)$; cf. Eq. (25). The apparent plateau in the long time limit of case (b) is due to the small value of k_u. The dashed line gives the slope at the origin and the dotted line for the apparent value of the plateau is the fractional population of receptors in the bound state $k_b/(k_u + k_b) = 0.5$.

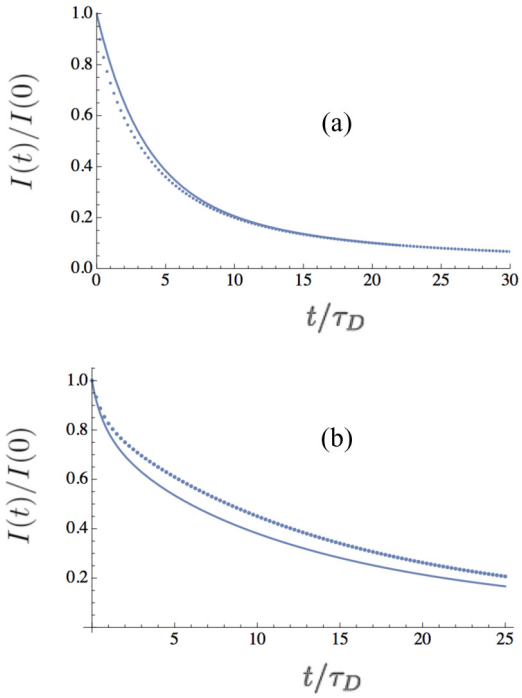

FIG. 7. Plots of the autocorrelation functions in different regimes according to Fig. 2. Case (a) corresponds to the dotted diagonal of Fig. 2 with $k_+\tau_D = k_-\tau_D = 0.5$. The continuous line is $I_0(t)$ of Eq. (21). In case (b), $k_b\tau_D = k_u\tau_D = 0.2$, and we have applied Eq. (24) for $I_1(t)$ (continuous line).

which differ from the result of Michelman-Ribeiro [15] by a few percent in this limit. The exponential factor $\exp[-k_u t]$ is responsible for the apparent plateau in the long time limit for case (b) of Figs. 6 and 7. This asymptotic form satisfies to condition Eq. (19) as evidenced by the coincidence of the two plots of Figs. 6 and 7. This asymptotic form also makes apparent that pure diffusion dominates the correlation function in the small t limit but that reaction gives the dominant behavior for larger $t \gg \tau_D$. This expression is simply interpreted. The factor $k_b^\star/(k_u + k_b^\star)$ accounts for the fractional population of receptors bound to a ligand with a residence time $1/k_u$, and this term dominates in the long time limit when k_u is small compared with $1/\tau_D$. This is the characteristic property of the hybrid regime.

VI. STOCHASTIC MODELING

For a small number of molecules, every chemical scheme such as Eqs. (3) and (4) is probabilistic per nature [18] and can be rewritten in terms of occupancy probabilities for compartments paving the 2D plane simulating the membrane; see Fig. 8. When this probability distribution is generated by stochastic numerical methods we can calculate the autocorrelation functions by sampling the system over enough time. All information is contained in the joint probability distribution for observing $n_{\uparrow,\downarrow,b}(x_i)$ molecules in the compartment i. I will employ a compartment-based version of Gillespie's algorithm, which implements stochastic modeling of a diffusion reaction process [19]. Each compartment is considered as homogeneous and compartments are coupled via diffusion. An event is a chemical reaction taking place in a box or a stochastic jump from one compartment to one of its neighbors. In the Gillespie algorithm, kinetic rate constants are conditional transition probabilities per time unit. From the sum of rates, the algorithm generates the distribution of times for the next event and each event is simulated with a probability proportional to its relative propensity.

To illustrate this method, it is useful to consider Fig. 3 and to represent the number of immobile integrins as a density plot. In this example, the algorithm generates the probability distribution for an equivalent biochemical scheme of Eqs. (3) and (4). Introducing a finite density of ligands as a model parameter, I consider systems of 50×50 boxes with a given number of ligands per compartment. As before, I will consider reflective and open boundary conditions.

Defining the equivalent illuminated surface as the partial sum over a subset S of N boxes, the weighted time correlation function equivalent to Eq. (5) is

$$I(t) = \sum_{i,j\in S} \langle n(i,t_0)n(j,t_0+t)\rangle_{t_0}, \tag{26}$$

where the "intensity" $n(i,t_0)$ is the sum of the number of free and ligated receptors in compartment i,

$$n(i,t_0) = n_\uparrow(i,t_0) + n_\downarrow(i,t_0) + n_b(i,t_0). \tag{27}$$

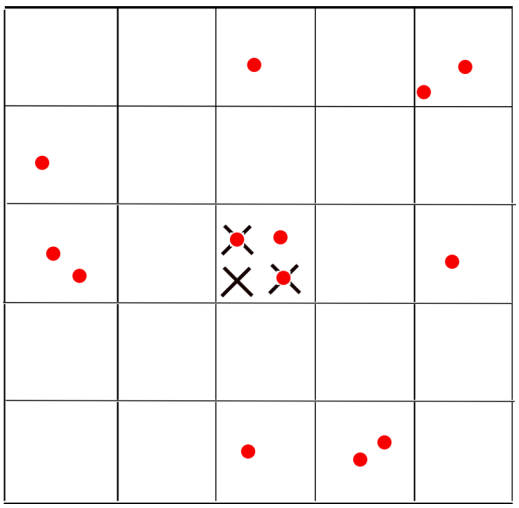

FIG. 8. Schematic of the compartment-based model used in the stochastic simulation. The system of size L is divided into $L/h \times L/h$ compartments playing the role of pixels. Diffusing receptors (red dots) can jump from one compartment to its neighbor with a rate D/h^2, where D is the continuous space diffusion constant. Each compartment is treated as an homogenous system where interaction between molecules occurs according to first-order kinetics. Crosses schematize fixed ligand molecules, the spatial distribution of which is to choose to mimic the contact area. In the simulation presented Fig. 3, 20 ligand molecules are distributed in the compartments located near the center to mimic a circular illuminated volume. Compartments located at the boundaries of system $x, y = -10, +10$ are periodically reshuffled with a multinomial distribution to mimic an infinite reservoir.

The subset S plays an equivalent role of the characteristic width w of the illuminated region and the partial sum in Eq. (26) corresponds to the circular case of the preceding section. Compared with the Gaussian cases that necessitate updating partial sums, this is the fastest numerical method to update, store, and save data while running the program. To compute the correlation functions, we update Eq. (26) at each time step and record the result if the new sum differs from the preceding one. The time interval between two events is also stored so that mean values and the variance can be computed separately by considering $I(t)$ as a stochastic variable.

As before, it is useful to define the diffusion time over the equivalent illuminated area. For a subset of N compartments in S, Nh^2/π is the square of the equivalent disk radius. Thus,

$$\tau_D = \frac{Nh^2}{\pi D}, \tag{28}$$

where D/h^2 is the renormalized diffusion coefficient for a compartment of size h used in the stochastic simulator. In what follows, Eq. (28) serves as a suitable reference time for our simulations, since Fig. 9 demonstrates that we recover the $1/(1 + t/\tau_D)$ law for free diffusing molecules.

Finally, since each compartment is treated as homogeneous, the diffusion coefficient must obey

$$D/h^2 \geqslant k_b^\star + k_u, \tag{29}$$

where $k_b^\star$ is taken as its mean-field value, $k_b^\star = k_b l_0$.

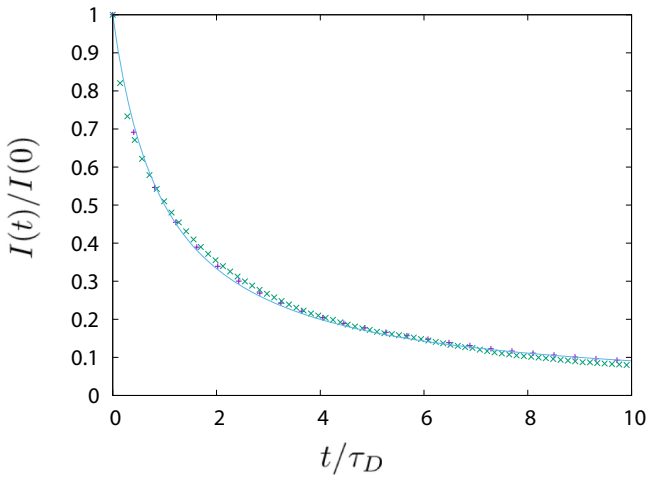

FIG. 9. Plot of the autocorrelation functions in the free diffusion limit. The two sets of data are renormalized by Eq. (28) and collapse on the universal $1/(1 + x)$ curve ($w^2 = 16,52$ compartments). Numerical corrections are only perceptible at very short time where the numerical tangent is vertical.

To illustrate the numerical method, it is appropriate to go beyond the mean-field approximation and to take into account fluctuations in ligand concentration. The stationary solutions of Eqs. (3) and (4) are easily found by solving an algebraic system. Let $n_{\downarrow,0}, n_{l,0}, l_0$ be these solutions. The fluctuations obey to linear order an equivalent system,

$$\partial_t \delta n_\downarrow = D\delta\Delta n_\downarrow - k_b l_0 \delta n_\downarrow + (k_u + k_b n_{\downarrow,0})\delta n_b, \tag{30}$$

$$\partial_t \delta n_b = +k_b l_0 \delta n_\downarrow - (k_u + k_b n_{\downarrow,0})\delta n_b, \tag{31}$$

where we have made use of mass conservation $\delta l = -\delta n_\downarrow$. Since the system has the same functional form as for reflective boundary conditions, it is easy to transcribe the preceding results using effective rate constants ($k_{u,\mathrm{eff}} = (k_u + k_b n_{\downarrow,0})$, $k_{b,\mathrm{eff}} = k_b^\star$).

Figure 10 presents our numerical date for the receptor correlation function in the three cases of small, equal, or large ligand concentration compared to receptor concentration. The from the top to the bottom, the ratio between the two concentrations varies from 1.5 to 0.5 with reflective boundary conditions. First, the strong dissimilarities between the plots and the fast convergence to the zero slope regime suggest that the asymptotic limit of large excess easily reached. Second, comparison with the mean-field data demonstrates that our preceding results remain valid for a small number of molecules but with appropriate effective rate constants as defined in Eqs. (30) and (31). Redefinition of rate constants due to ligand fluctuation may, however, alter the interpretation strongly of the autocorrelation function as the sum of two parts, one for the free and the other one for the bound fraction of receptors. This is also illustrated in Fig. 11 where we recover the long time tail limit of the small k_u hybrid regime. For all these curves with equal number of ligands and receptors, almost all ligands are bound to receptors with a very small fraction of free receptors in marked contrast with the naive $1/2$ result suggested by the plots.

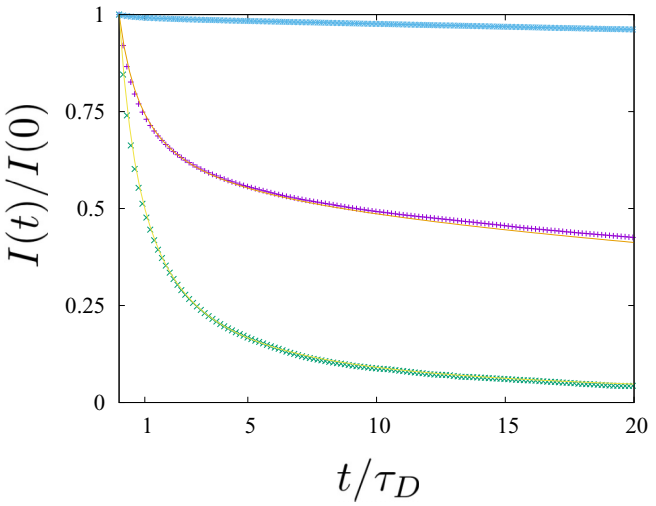

FIG. 10. Plots of the autocorrelation functions for different values of ligands and receptor densities. From the top to the bottom curve L = 30, 20, 10, with an average of 20 receptors per compartment ($k_b = 10^{-3}$, $k_u = 5.0\,10^{-5}$). The thin lines correspond to the mean-field result using effective rate constants as explained in the text; see Eqs. (30) and (31) with Eq. (25). Data correspond to reflective boundary conditions.

VII. EFFECT OF NOISE

The usefulness of the stochastic simulator is to allow us to consider limits where neither ligands nor receptors are in excess. It is also the only way to study the biologically relevant problem of noise due to environmental fluctuations. For the receptor-ligand situation, this problem arises naturally when the number of ligands in each elementary compartment is a stochastic variable.

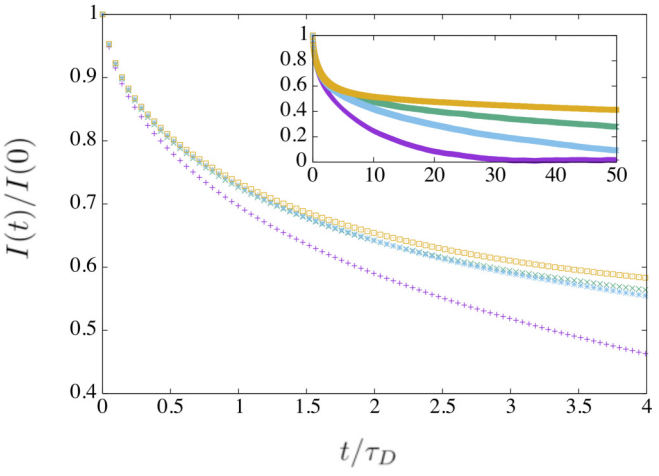

FIG. 11. Plot of the receptor correlation function $\langle \delta n(t)\delta n(0)/\delta n(0)^2\rangle$ in the hybrid regime of part I. These plots evidence the presence of two time scales in the small and long time limit. The short time limit is characterized by the effective diffusion time defined in Eq. (19). The long time limit exhibits, however, an apparent plateau when k_u is sufficiently small. From the top to the bottom, $k_u = 5.0\,10^{-a}$, $a = 7, 6, 5, 4$, with $k_b = 10^{-3}$. For these simulations, the average number of ligands per cell equal the average number of receptors per cell, i.e., 20 (reflective boundary conditions).

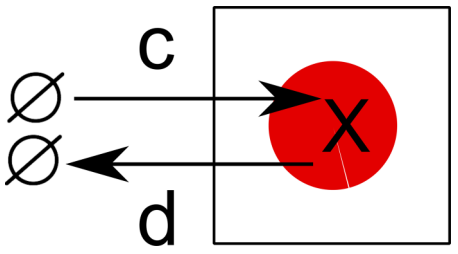

FIG. 12. Figure illustrating the birth and death process by which immobile ligands with symbol X are created with rate c and destroyed with rate d in the adhesive disk; see Eq. (32). I–L complexes are snapped with same probability.

To investigate this effect we can generalize the preceding model by adding point (c) to points (a) and (b) as follows. (a) Receptor I have two conformational states, $I_\uparrow$, $\downarrow$, and diffuse on the membrane with diffusion constant $D_{\uparrow,\downarrow}$, respectively. (b) Receptors in state $\downarrow$ bind and unbind from ligands with rates $k_{b,u}$. Receptors bound to ligands form a complex I − L. Receptors in state $\uparrow$ cannot bind to ligands. (c) The number L of free ligands is a stochastic variable and follows the statistics of a molecule experiencing a birth-death process, which controls their number and their lifetime. This scheme can be summarized as follows, see Fig. 12:

$$\begin{array}{c} \varnothing \underset{\mathrm{d}}{\overset{\mathrm{c}}{\rightleftarrows}} \mathrm{L} \\ \mathrm{I}-\mathrm{L} \xrightarrow{\mathrm{d}} \mathrm{I}_\downarrow \end{array}, \tag{32}$$

where c and d are kinetics rates for creation and destruction. The ratio c/d fixes the mean density of ligands by $\langle \mathrm{L}\rangle = \mathrm{c/d}$. This ratio is constant under rescaling of both c and d. Thus, varying c and d at constant ratio interpolates between a fast fluctuating regime compared with the integrin binding-unbinding cycle and a slow turnover regime where integrins experience many cycles before a change in the number of ligands takes place.

A first point is that these fluctuations regulate the number of integrin-ligand complexes by a simple mechanism. The plots of Fig. 13 give the instantaneous number of complexes $\mathrm{I}_\downarrow - \mathrm{L}$ in a region of width w for three typical numerical runs all starting at time 0 with the same initial condition with zero complex $\mathrm{I}_\downarrow - \mathrm{L}$. The ratio c/d being the same in the three cases, the average ligand concentration is the same for all plots with the top curve corresponding to a slow and the bottom one to a fast ligand turnover. After a transient period of time corresponding to the first binding-unbinding events, all the three curves sample their stationary distribution and fluctuate around their mean. Increasing the dynamics for the fluctuations of the number of ligands L leads to the following observations. (a) The mean number of receptor-ligand complexes I–L decreases with increasing c and d at fixed ratio c/d. (b) The fluctuations in the number of I − L do not scale with the mean as they do if statistics were Poissonian, i.e., $\langle \delta n^2\rangle \propto \langle n\rangle$. Point (a) is easily understood, since if the number of ligands varies to rapidly in each compartment, only a small subset of them can form a complex with the receptors. The limit of very fast turnover of ligand is thus equivalent to the large unbinding

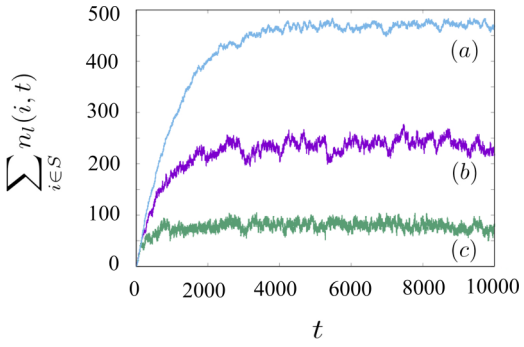

FIG. 13. Number of receptor-ligand complexes I−L in a circular domain of size $w^2 = 52$ compartments. The time $t = 0$ coincides with initial conditions with zero number of ligand-receptor complexes. The three cases shown correspond to slow (top curve) and fast ligand turnover. After a transient period the number of ligand-receptor pairs fluctuate around a mean and the mean decreases with increasing this rate. (a) $5.0\,10^{-3}\mathrm{s}^{-1}$, (b) $10^{-2}\mathrm{s}^{-1}$, (c) $5.0\,10^{-2}\mathrm{s}^{-1}$.

rate limit for receptor-ligand complexes and it matches in an asymptotic way the free diffusion limit.

Compared with what precedes, the intrinsic noise due to conformational changes of receptors has a minor effect. Here, the short time limit of the correlations is fixed by diffusion of non-activated receptors. This point is also illustrated in Fig. 14, which demonstrates that correlations decrease as the turnover

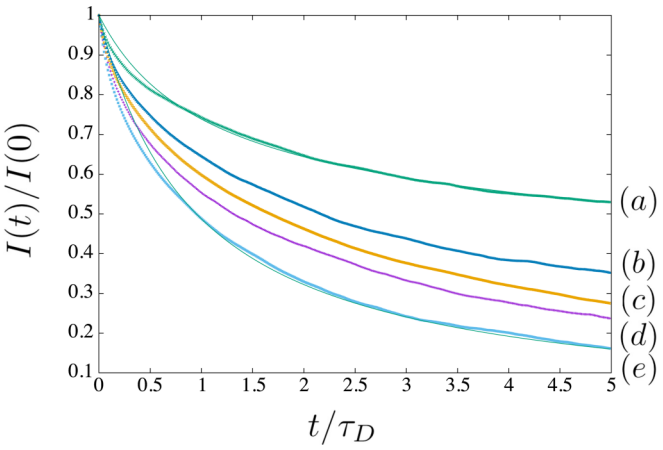

FIG. 14. Correlation function for the total number of receptors [Eq. (27)] in a circular domain of size $w^2 = 52$ compartments. From the top to the bottom curve, the characteristic rate for the fluctuations of the number of ligands per compartment increases. When this rate is large enough, the system is equivalent to the pure diffusion case (continuous blue line at the bottom). For a slower rate, top curve, correlations regress according to Eq. (25) with a long time tail (top continuous line in green adjusted to the mean filed value $k_b^\star = k_b\langle \mathrm{L}\rangle$). The characteristic frequency at which the system crosses over to the pure diffusive regime corresponds to the frequency of the binding-unbinding cycle of a receptor with its ligand ($k_b^\star = k_u = 0.01\,\mathrm{s}^{-1}$). Top curve (a) $5\,10^{-4}\,\mathrm{s}^{-1}$, (b) $5.0\,10^{-3}\,\mathrm{s}^{-1}$, (c) $7{,}5\,10^{-3}\,\mathrm{s}^{-1}$, (e) $5.0\,10^{-2}\,\mathrm{s}^{-1}$, the continuous line almost coinciding with curve (e) corresponds to the pure diffusion problem. The effective diffusion constants for activated and nonactivated integrins are $0.1/\mathrm{h}^2$ and $0.05/\mathrm{h}^2$, where h is the compartment size. The apparent slope at the origin is 1 as stated in the text. Data correspond to open boundary conditions.

of ligands increases. In the large turnover regime, fluctuations and means in the number of integrins are therefore controlled by the number of ligands and not by diffusion nor reaction. This shows that not only spatial fluctuations of ligands but also the characteristic time scale impacting the cadence at which ligands appear and disappear is an efficient way to regulate adhesive complexes.

VIII. DISCUSSION AND CONCLUSION

Visualizing protein dynamics to characterize localization and adhesion turnover by a range of microscopy techniques calls for a better modeling of the first events following immobilization and engagement of integrin receptors in adhesion sites. This work presents a quantitative study for the time correlations for receptors subject to diffusion and to reaction immobilization. Other approaches such as FRAP analysis [20] give rate constants, but we have shown that correlation spectroscopies give information on molecular concentrations. The principal result formulated in Fig. 2 is the presence of an hybrid domain for a large set of rate constants where diffusion and reaction cannot be considered as separable processes. The landmark of this regime is a rapid decrease of the correlation at short times followed by a long exponential tail when diffusion and reaction operate at very different time scales. Stochastic simulations have shown that this regime survives in more realistic models with multiconformational states for receptors and subject to environmental noise such as time fluctuations in the number of ligands serving as substrate immobilizing the receptors.

In living cells, the nanoscale dynamics of integrin receptors in adhesive sites results from a complex hierarchy of processes involving extra and intracellular factors. External ligand binding of receptor triggers integrin clustering and integrin-actin linkages [21]. These linkages are finely regulated through proteins such as talin and covalent modifications [22]. It is likely that these processes may not result in one but rather in a broad distribution of residence times which are typically larger than the diffusion time of a receptor [5,23]. Under the general assumption of statistical independence, the resulting receptor autocorrelation function is the averaged autocorrelation function over the distribution of residence time and the results derived in this paper may apply.

ACKNOWLEDGMENTS

I thank R. de Mets and C. Albigès-Rizzo for insightful comments during preparation of this manuscript. I am very indebted to O. Destaing and A. Delon for sharing their insights and for their useful suggestions and comments.

APPENDIX

1. Notations in the Gaussian case

In the Gaussian case, the following integral gives the correlation function:

$$I(t) = \int_0^\infty k dk\, e^{-k^2}\big[(\alpha_{11}+\alpha_{21})\langle \delta n_\downarrow^2\rangle \tag{A1}$$

$$+ (\alpha_{12}+\alpha_{22})\langle \delta n_b^2\rangle\big]. \tag{A2}$$

For reflective boundary conditions, the stationary solutions are given in terms of the free and bound fractions,

$$\langle \delta n_\downarrow^2 \rangle = \langle n_\downarrow \rangle = k_u/(k_b^\star + k_u), \tag{A3}$$

$$\langle \delta n_b^2 \rangle = \langle n_b \rangle = k_b^\star/(k_b^\star + k_u). \tag{A4}$$

For open boundary condition, we have $\langle \delta n_\downarrow^2 \rangle = \langle n_\downarrow \rangle = n_e$, where n_e is fixed by the reservoir. In this case, n_b must be calculated as in the text. It is also convenient for typographic reasons to use the notation

$$D_e = 1/\tau_D, \tag{A5}$$

so that D_e has the dimension of the inverse of a time. The k appearing in Eq. (A1) are dimensionless quantities.

Result 1

Let $(1, b_\pm)$ be the eigenvectors associated with the eigenvalues $\Lambda_\pm(k)$. Define

$$\Delta(k) = (k_b^\star + k_u + D_e k^2)^2 - 4k^2 D_e k_u. \tag{A6}$$

We have

$$\Lambda_\pm(k) = \tfrac{1}{2}[-(k_b^\star + k_u + D_e k^2) \pm [\Delta(k)]^{1/2}] < 0, \tag{A7}$$

with

$$b_+ = [\Lambda_+ + k_b^\star + D_e k^2]/k_u, \tag{A8}$$

$$b_- = [\Lambda_- + k_b^\star + D_e k^2]/k_u. \tag{A9}$$

The matrix elements $\alpha_{i,j}$ appearing in Eq. (A1) are functions of k and t:

$$\alpha_{11} = (b_+ \exp[\Lambda_- t] - b_- \exp[\Lambda_+ t])/(b_+ - b_-), \tag{A10}$$

$$\alpha_{12} = (\exp[\Lambda_+ t] - \exp[\Lambda_- t])/(b_+ - b_-), \tag{A11}$$

$$\alpha_{21} = -b_- b_+ \alpha_{12}, \tag{A12}$$

$$\alpha_{22} = (b_+ \exp[\Lambda_+ t] - b_- \exp[\Lambda_- t])/(b_+ - b_-). \tag{A13}$$

For what follows, it will be useful to consider the two functions:

$$I_\pm(t) = 2\int_0^\infty dk\, k C_\pm(k) \exp[-k^2 + \Lambda_\pm(k) t], \tag{A14}$$

where $C_\pm(k)$ are functions of the α_{ij}'s. In the notations of Ref. [15], we find

$$C_-(k) = \tfrac{1}{2}[1 - \phi(k)], \tag{A15}$$

$$C_+(k) = \tfrac{1}{2}[1 + \phi(k)], \tag{A16}$$

with

$$\phi(k) = \frac{1}{\sqrt{\Delta(k)}}\left[k_b^\star + k_u + \frac{k_b^\star - k_u}{k_b^\star + k_u} D_e k^2\right]. \tag{A17}$$

A direct calculation shows that

$$I(t = 0) = 1, \tag{A18}$$

since

$$I(t = 0) = I_+(0) + I_-(0) = 1. \tag{A19}$$

Using the functional form given above, the following limits are useful to discuss the small and large $k_b^\star \tau_D$ limits,

$$\lim_{k\to 0} \phi(k) = 1 \quad \lim_{k\to+\infty} \phi(k) = \frac{k_b^\star - k_u}{k_b^\star + k_u}. \tag{A20}$$

For open boundary conditions, the expression of $C_\pm(k)$ must be recalculated using Eq. (A10) with analogous properties.

2. General properties

a. Result 1

From Eq. (A7), the two eigenvalues behaves in the limit $k \ll 1$ as

$$\Lambda_+(k) \simeq -\frac{k_u}{k_b^\star + k_u} D_e k^2, \quad k \ll 1, \tag{A21}$$

$$\Lambda_-(k) \simeq -(k_b^\star + k_u) - \frac{k_u}{k_b^\star + k_u} D_e k^2, \quad k \ll 1. \tag{A22}$$

In the other limit, $k \gg 1$, $\Lambda_+(k)$ tends to off rate for unbinding k_u, but $\Lambda_-(k)$ is unbounded,

$$\Lambda_-(k) \simeq -D_e k^2, \quad k \gg 1, \tag{A23}$$

$$\Lambda_+(k) \simeq -k_u + \frac{k_b^\star k_u}{D_e k^2}, \quad k \gg 1. \tag{A24}$$

Thus, $\Lambda_+(k)$ is steplike, but $\Lambda_-(k)$ is parabolic with for any k

$$\Lambda_-(k) < \Lambda_+(k) < 0. \tag{A25}$$

It is also useful to consider the derivative of $I(t)$ in Eq. (A1). From definition Eq. (A10), the $\alpha_{i,j}$'s are functions of t. Taking the derivative with respect to t is straightforward. For $t = 0$, algebra shows:

b. Result 2

$$\frac{d}{dt}\left[(\alpha_{11} + \alpha_{21})\langle \delta n_\downarrow^2 \rangle + (\alpha_{12} + \alpha_{22})\langle \delta n_b^2 \rangle\right]\Big|_{t=0} = -D_e k^2 \frac{k_u}{k_b^\star + k_u}, \tag{A26}$$

from which we get

$$I'(t) = -D_e k_u/(k_b^\star + k_u) \tag{A27}$$

as quoted in the text. For open boundary conditions, a similar calculation gives $-D_e$.

3. Comparison with the sharp circular case

For a circular hole, we substitute

$$\int d^d x e^{-2x^2/w^2} e^{i\mathbf{k}.\mathbf{x}} \to \int_{\Omega(w)} d^d x e^{i\mathbf{k}.\mathbf{x}}. \tag{A28}$$

We have

$$\int_0^{2\pi} d\theta e^{ikr\cos\theta} = 2\pi J_0(kr) \tag{A29}$$

and

$$\int_0^w dr\, r J_0(kr) = \frac{w}{k} J_1(kw), \tag{A30}$$

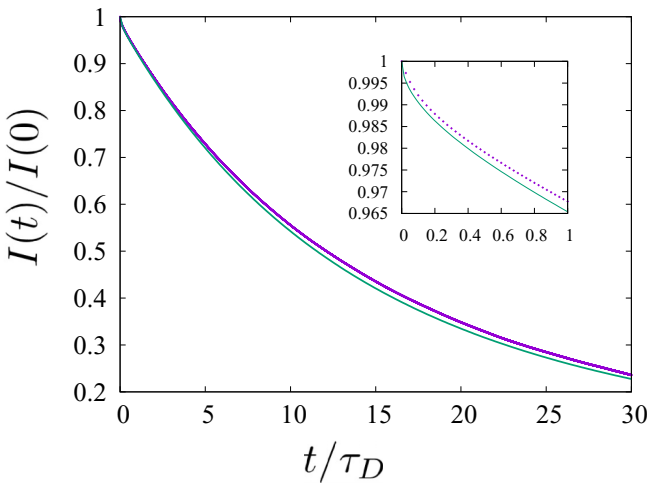

FIG. 15. Plot of the correlation function for a sharp circular illuminated domain as a function of t/τ_D. The doted line is the result of a stochastic simulation and the continuous line is a fit using reflective boundaries and a sharp circular domain. The inset details the neighborhood of the origin where the tangent is parallel to the vertical axis for both curves ($w^2 = 3$ (52 pixels), $k_b^\star = 0.02$ and $k_u = 0.001$).

and we find

$$I(t) = (4\pi)^2\omega^2 \int_0^\infty dk\, \frac{1}{k} J_1^2(k\omega)\big[(\alpha_{11}+\alpha_{21})\langle \delta\tilde{n}_\downarrow^2\rangle + (\alpha_{22}+\alpha_{12})\langle \delta\tilde{n}_b^2\rangle\big]. \tag{A31}$$

Pure diffusion leads to the integral

$$I(t)/I(0) = 2\int_0^\infty \frac{dq}{q} J_1^2(qw) e^{-Dq^2 t}. \tag{A32}$$

In the limit $t \to \infty$, we can expand the Bessel function $J_1(x) \simeq x/2 + \ldots$ and the previous integral gives

$$1/4Dt, \tag{A33}$$

so that circular diffusion autocorrelation function have the same asymptotic behavior as $t \to \infty$, as the Gaussian circular autocorrelation function.

To evaluate the derivative of $I(t)$, we differentiate directly Eq. (A31) under the integral sign and retain the dominant power for the wave vector k. This leads us to evaluate integral

$$\int_0^\infty dk\, k J_1(k)^2, \tag{A34}$$

which diverges in the small wavelength limit. Thus, we have shown that the slope of $I(t)$ in the circular case must be tangent to the vertical axis. As seen in Fig. 15, the numerical simulations reproduce correctly this result.

4. Some results

a. Result 1

We evaluate the integral

$$I_0(t) = 2\int_0^\infty dk\, k e^{-k^2+\Lambda_+(k)t}. \tag{A35}$$

Since $\Lambda_+(k)$ is a strictly decreasing function of k, the inverse function $k(\Lambda_+)$ is well-defined. We make the change of variable $k \to \Lambda_+(k)$ in Eq. (A14). Defining $a = k_b^\star + k_u$, we get

$$I_0(t) = -\int_0^{-k_u} du\, \frac{d}{du}\left[\frac{u(u+a)}{D_e(k_u+u)}\right] \times \exp\left[\frac{u(u+a)}{D_e(k_u+u)}\right]\exp[ut], \tag{A36}$$

which is integrated by parts with the change of variable $u \to -u$,

$$I_0(t) = 1 - t\int_0^{k_u} du\, \exp\left[-\frac{k_b^\star}{D_e}\frac{u}{k_u-u}\right] \times \exp[-u(t+\tau_D)]. \tag{A37}$$

Because of the first exponential, the integral is dominated by the neighborhood of the origin. Expanding the second exponential, the integral becomes a series,

$$I_0(t) = 1 - t\sum_{n\geqslant 0}\frac{(-1)^n}{n!}\int_0^{k_u} du\, \exp\left[\frac{k_b^\star}{D_e}\frac{u}{k_u-u}\right] u^n (t+\tau_D)^n. \tag{A38}$$

Next, we make the change of variable

$$s = u/(k_u - u) \tag{A39}$$

and get

$$I_0(t) = 1 - k_u t\sum_{n\geqslant 0}(-1)^n (t+\tau_D)^n k_u^n U(1+n,0,k_b^\star\tau_D), \tag{A40}$$

where $U(a,b,z)$ is a special function (hypergeometric U); see Ref. [24].

b. Result 2

We have

$$I(t) = I_+(t) + I_-(t), \tag{A41}$$

where we have defined

$$I_\pm(t) = 2\int_0^\infty k C_\pm(k) e^{-k^2+\Lambda_\pm(k)t}. \tag{A42}$$

In this section, we show the following:

$$I_+(t) + I_-(t) \simeq \frac{k_b^\star}{k_b^\star+k_u} I_0(t) + \frac{k_u}{k_b^\star+k_u}\frac{1}{1+t/\tau_D}, \tag{A43}$$

when

$$(k_u + k_b^\star)\tau_D \ll 1. \tag{A44}$$

In practice, Eq. (A43) works well even if Eq. (A44) approximately holds; see case (a) of Figs. 6 and 7.

(1) We split $I_+(t)$ in two as follows:

$$I_+(t) = 2\int_0^{+\infty} dk\, k C_+(k) e^{-k^2+\Lambda_+(k)t} \simeq 2\int_0^{q_i^{\star\star}} dk\, k(C_+(0) - C_+(\infty)) e^{-k^2+\Lambda_+(k)t} + 2\int_0^{+\infty} dk\, k C_+(\infty) e^{-k^2+\Lambda_+(k)t}, \tag{A45}$$

where the inflexion point $q_i^\star$ is defined in Eq. (18). We have

$$C_+(0) = 1 \quad C_+(\infty) = \frac{k_b^\star}{k_b^\star + k_u}. \tag{A46}$$

The first integral is easily evaluated as

$$\frac{k_u}{k_b^\star + k_u} \frac{1}{1 + t/\tau_D} \left[1 - e^{-q_i^2(1+t/\tau_D)}\right], \tag{A47}$$

and the second integral is simply the definition of $I_0(t)$; see Eq. (A35).

(2) In this regime, $I_-(t)$ can be evaluated in a similar way. We have

$$C_-(0) = 0 \quad C_-(\infty) = \frac{k_u}{k_b^\star + k_u} \tag{A48}$$

so

$$I_-(t) \simeq \frac{k_u}{k_b^\star + k_u} \frac{1}{1 + t/\tau_D} e^{-q_i^2(1+t/\tau_D)}. \tag{A49}$$

Summing both contribution Eqs. (A45) and (A49), the exponential term cancels out and we get Eq. (A43).

c. Result 3

It is useful to derive the asymptotic expansion of Eq. (A35) in two limit cases. We use formula (13-5-11) and (13-5-2) of Ref. [24],

$$U(1 + n, 0, z) \approx 1/(n + 1)!, \quad z \ll 1, \tag{A50}$$

$$U(1 + n, 0, z) \approx 1/z^{n+1}, \quad z \gg 1, \tag{A51}$$

which leads to

$$I_0(t) \approx 1 - \frac{t}{t + \tau_D}[1 - e^{-k_u(t+\tau_D)}], \quad k_b^\star \tau_D \ll 1, \tag{A52}$$

$$I_0(t) \approx \left[1 + \frac{k_u}{k_b^\star + k_u} t/\tau_D\right]^{-1}, \quad k_b^\star \tau_D \gg 1. \tag{A53}$$

Using Eq. (A43), Eq. (A52) gives the asymptotic expansion stated in the text. In particular, $k_b^\star \tau_D \ll 1$ is compatible with condition Eq. (A44) so that

$$\begin{aligned} I(t) &= I_+(t) + I_-(t) \\ &\simeq \frac{1}{1 + t/\tau_D} + \frac{k_b^\star}{k_u + k_b^\star} \frac{t}{1 + t/\tau_D} \exp[-k_u t]. \end{aligned} \tag{A54}$$

Taking the derivative with respect to t at $t = 0$, this asymptotic form satisfies to the exact result Eq. (19) of the text. The exponential term in the first equation is responsible for the slow long tail limit seen in case (b) of Figs. 6 and 7 and the second equation corresponds the effective diffusion limit with a diffusion constant rescaled by the rate constants.

d. Result 4

In the other limit,

$$(k_b^\star + k_u)\tau_D \gg 1, \tag{A55}$$

we have

$$I(t) \simeq I_0(t). \tag{A56}$$

In practice, the last approximation works even if Eq. (A55) holds only approximately; see case (c) of Figs. 6 and 7.

[1] M. Weissman, Annu. Rev. Phys. Chem. **32**, 205 (1981).
[2] P. W. Wiseman, Methods Enzymol. **518**, 245 (2013).
[3] B. Kholodenko, Nat. Rev. Mol. Cell Biol. **7**, 165 (2006).
[4] B. N. Kholodenko, J. F. Hancock, and W. Kolch, Nat. Rev. Mol. Cell Biol. **11**, 414 (2010).
[5] P. W. Wiseman, C. M. Brown, D. J. Webb, B. Hebert, N. L. Johnson, J. A. Squier, M. H. Ellisman, and A. F. Horwitz, J. Cell Sci. **117**, 5521 (2004).
[6] C. M. Brown, B. Hebert, D. L. Kolin, J. Zareno, L. Whitmore, A. R. Horwitz, and P. W. Wiseman, J. Cell Sci. **119**, 5204 (2006).
[7] A. I. Bachir, J. Zareno, K. Moissoglu, E. F. Plow, E. Gratton, and A. R. Horwitz, Curr. Biol. **24**, 1845 (2014).
[8] K. Hu, L. Ji, K. T. Applegate, G. Danuser, and C. M. Waterman-Storer, Science **315**, 111 (2007).
[9] O. Rossier, V. Octeau, J.-B. Sibarita, C. Leduc, B. Tessier, D. Nair, V. Gatterdam, O. Destaing, C. Albigès-Rizo, R. Tampé, L. Cognet, D. Choquet, B. Lounis, and G. Giannone, Nat. Cell Biol. **14**, 1057 (2012).
[10] A. C. E. Shibata, T. K. Fujiwara, L. Chen, K. G. N. Suzuki, Y. Ishikawa, Y. L. Nemoto, Y. Miwa, Z. Kalay, R. Chadda, K. Naruse, and A. Kusumi, Cytoskeleton **69**, 380 (2012).
[11] O. Rossier and G. Giannone, Exp. Cell Res. **343**, 28 (2016).
[12] R. O. Hynes, Cell **110**, 673 (2002).
[13] F. Marks, U. Klingmüller, and K. Müller-Decker, *Cellular Signal Processing: An Introduction to the Molecular Mechanisms of Signal Transduction* (Garland Science, New York, 2009).
[14] R. Changede and M. Sheetz, Bioessays **39**, 1 (2017).
[15] A. Michelman-Ribeiro, D. Mazza, T. Rosales, T. J. Stasevich, H. Boukari, V. Rishi, C. Vinson, J. R. Knutson, and J. G. McNally, Biophys J. **97**, 337 (2009).
[16] M. Lax and P. Mengert, J. Phys. Chem. Solids **14**, 248 (1960).
[17] N. Van Kampen, *Stochastic Processes in Physics and Chemistry* (North-Holland, Amsterdam, 1981).
[18] G. Gardiner, *Handbook of Stochastic Processes for Physics, Chemistry, and Natural Sciences*, 2nd ed. (Springer Verlag, Berlin, 1985).
[19] R. Erban, J. Chapman, and P. Maini, A practical guide to stochastic simulations of reaction-diffusion processes, arxiv:0704.1908.
[20] B. L. Sprague, R. L. Pego, D. A. Stavreva, and J. G. McNally, Biophys J. **86**, 3473 (2004).
[21] C. Cluzel, F. Saltel, J. Lussi, F. Paulhe, B. A. Imhof, and B. Wehrle-Haller, J. Cell Biol. **171**, 383 (2005).
[22] K. R. Legate and R. Fässler, J. Cell Sci. **122**, 187 (2009).
[23] R. de Mets, Study of the Mechanotransduction: Relation between Cellular Traction Forces and Integrin Fynamics (in French), Ph.D. thesis, Thèse de doctorat en Physique pour les Sciences du Vivant, Grenoble-Alpes University, 2015.
[24] M. Abramowitz and I. Stegun, *Handbook of Mathematical Functions* (National Bureau of Standards, Gaithersberg, MD, 1964).